2

Erdman, Natasha, and Nicholas Drenzek, 2013, Integrated preparation and imaging techniques for the microstructural and geochemical characterization of shale by scanning electron microscopy, *in* W. Camp, E. Diaz, and B. Wawak, eds., Electron microscopy of shale hydrocarbon reservoirs: AAPG Memoir 102, p. 7–14.

Integrated Preparation and Imaging Techniques for the Microstructural and Geochemical Characterization of Shale by Scanning Electron Microscopy

Natasha Erdman

JEOL USA Inc., 11 Dearborn Rd., Peabody, Massachusetts, 01960, U.S.A. (e-mail: erdman@jeol.com)

Nicholas Drenzek[1]

Statoil Research Center, Sandsliveien 90, 5020-Bergen Norway. (e-mail: ndrenzek@statoil.com)

ABSTRACT

To better understand the influence of microscale geochemical and microstructural relationships on the bulk petrophysical properties of unconventional shale systems, core samples from four producing North American formations were cross-sectioned with an argon ion polisher and imaged with a field emission scanning electron microscope (FE-SEM) using a variety of complementary detectors. We demonstrate distinct advantages of the ion-polishing technique for the preservation of the internal shale structure. Moreover, we show how such preparation affords a wider choice of imaging options for both chemical and structural characterization, such as backscatter electron observation at varying beam potentials coupled with x-ray and cathodoluminescence spectroscopic techniques.

INTRODUCTION

Gas and oil production from shale formations has become an increasing component of North American energy supply over the past ten years and may likewise rebalance the global energy portfolio in the coming decade. The fundamental microstructural and geochemical properties of shales differ markedly from traditional petroleum reservoirs, however, presenting significant technical challenges that today hinder full exploitation. Two of the more important differences lie in the small dimension and mixed wettability of their pore network (Passey et al., 2010), characteristics that themselves arise from the abundant micrometer- to nanometer-size clay mineral grains and organic matter macerals interspersed throughout more conventional carbonate or sandstone matrices. Not surprisingly, then, the application and interpretation of many conventional analysis techniques such as mercury intrusion porosimetry have proven to be more complex for

[1] *Previous address: Schlumberger-Doll Research, 1 Hampshire St., Cambridge, Massachusetts, 02139, U.S.A.*

DOI: 10.1306/13391700M1023581

Table 1. Alphabetical List of Common Acronyms Used in This Text

Acronym	Full Name
BSE	backscattered electron
CL	cathodoluminescence
CP	cross-section polisher
EA	elemental analysis
EDS	energy-dispersive spectroscopy
FE	field emission
PMT	photomultiplier tube
SDD	silicon drift detector
SE	secondary electron
SEM	scanning electron microscopy
TOC	total organic carbon
VR_O	vitrinite reflectance
VR_E	vitrinite reflectance equivalent
XRD	x-ray diffraction

such critical petrophysical data in organic matter- and clay mineral-rich shale reservoirs (e.g., Dacy, 2010).

Scanning electron microscopy (SEM; see Table 1 for a list of most of the acronyms used in this chapter), is well suited to study the complex distribution and association of organic, mineral, and pore phases at the nanoscale that govern multiphase fluid transport in shale formations. The application of onboard backscattered electron (BSE), energy dispersive spectroscopy (EDS), and cathodoluminescence (CL) detectors to ion cross-polished sample surfaces has opened an unparalleled window into such rock "fabric" (Ogura et al., 2007; Bustin and Bustin, 2008; Loucks et al., 2009; Wang and Reed, 2009; Curtis et al., 2010; Loucks et al., 2010; Milner et al., 2010; Sondergeld et al., 2010; Curtis et al., 2011a, b), which is in turn critical to describing the pore saturations, flow mechanisms, and production rates of fluids therein (O'Brien et al., 1994, 2002; Javadpour et al., 2007; Javadpour, 2009; Loucks et al., 2009; Ross and Bustin, 2009; Wang and Reed, 2009; Shabro et al., 2011; Sun et al., 2011). This chapter seeks to review the state of the art in such SEM preparation and analysis techniques for shales through a comparative case study of samples collected from several producing North American gas shale plays.

METHODS

Cores from the Marcellus, Haynesville, Woodford, and Barnett formations were collected, slabbed, subsampled into aliquots of millimeter-size fragments from 5-cm (1.9685-in.) depth intervals, split, and further pulverized for analysis (Table 2). Bulk density was measured using the Archimedes method. Values for porosity (ϕ) were acquired via gas intrusion (Handwerger et al., 2011) and total organic carbon (TOC) contents were measured by combustion elemental analysis (EA) following carbonate removal using the HCl fumigation method (Brodie et al., 2011). Thermal maturity T_{max} values were acquired by Rock-Eval pyrolysis (Behar et al., 2001), while vitrinite reflectance (VR_O), and bitumen reflectance (VR_E) measurements were obtained using standard organic petrology methods (Schieber, 2001). Mineralogy was measured by x-ray diffraction (XRD) (Ruessink and Harville, 1992).

Similar to established optical petrology techniques, several milligrams of pulverized material from the same aliquots used for bulk measurements were embedded in epoxy resin to mechanically stabilize them and polished using a broad argon ion beam cross-section polisher (CP) normal to the intended SEM imaging direction at 5 kV for 4 h. This workflow produced a typical cross-sectioned area of 1.5 × 0.5 mm with minimal smearing or deformation (Figure 1) (Erdman et al., 2006a, b; Ogura et al., 2007; Loucks et al., 2009; Sondergeld et al., 2010). Whereas any features of the native shale fabric beyond the 150-μm window were compromised through pulverization, those

Table 2. Bulk geophysical and geochemical characteristics for samples under study

Sample	ρ_B (g/cm^3)	ϕ	*TOC*	R_O (%)	T_{MAX} (°C)	*Quartz*	*Carbonate*†	*Clay*§	*Pyrite*
Marcellus	2.57	6.5	11	2.0	501	24	10	51	8
Haynesville	2.41	11.8	5	2.4*	512	27	34	29	4
Woodford	1.93	4.8	23	0.6	435	25	9	48	7
Barnett	2.47	3.9	5	0.6	441	58	38	4	1

†Calcite + dolomite + ankerite.
§Illite + smectite + kaolinite + chlorite + biotite + glauconite + muscovite.
*Solid pyrobitumen value.

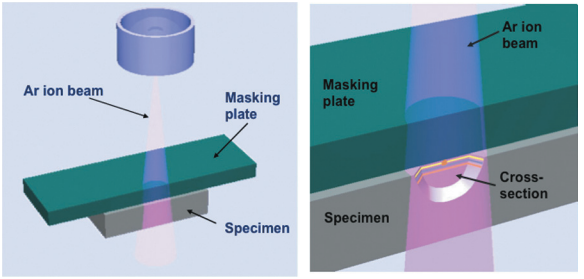

Figure 1. Principle of CP (cross-section polisher) operation. A specimen is masked so that a small portion (few tens of micrometers) protrudes from the mask. The exposed area is ablated with the argon ion beam and results in a specimen cross section with minimal artifacts.

viewed within the fragments less than 150 μm themselves should remain representative at this smaller scale. The resulting surfaces were then coated with less than a 100-Å thick elemental carbon film via vacuum evaporator to mitigate charge buildup and were examined with a Schottky field emission scanning electron microscope (FE-SEM) under high vacuum (10^{-4} Pa) using beam-accelerating voltages of 8 and 2 kV and a high-resolution, low-angle detector. Corresponding EDS elemental maps were then obtained using a 50-mm^2 silicon drift detector (SDD) at 8 kV for three frames (289 s per frame) with drift correction engaged. High-resolution CL and companion grayscale BSE images were also acquired using a FE-SEM system with a KE Centaurus CL detector containing a photomultiplier tube (PMT) set to detect photons in the 185- to 850-nm range.

RESULTS AND DISCUSSION

Cross-section polishing is an indispensable advancement for fine-scale SEM investigations of the distributions and associations of organic matter, minerals, and pores in highly consolidated geologic samples. Because major shale constituents such as organic matter, clay minerals, quartz, carbonate, and pyrite exhibit various degrees of hardness, traditional mechanical preparation (saw cutting, grinding, abrasive polishing, microtome cutting, etc.) tends to result in uneven surfaces as a result of smearing and/or pitting. Figure 2 shows an example of a Marcellus shale specimen polished with silicon carbide 1200-grit paper versus the same sample after CP preparation. The comparison clearly demonstrates that inappropriate sample preparation will confound subsequent attempts to image the exact locations of organic matter macerals and mineral grains along with both their internal and interfacial pore networks. In a study comparing native versus CP prepared surfaces, Milner et al. (2010) likewise concluded that such assessments of shale fabric are impossible without CP pretreatment.

Figure 3 shows relatively low magnification overview BSE images of CP prepared samples from the four formations investigated here. Backscatter images tend to provide better visualization of the various components of shale samples for two reasons: (1) the polished samples are very flat, thus providing minimal topography and relief-based contrast on which secondary electron (SE) images rely for interpretation, and (2) the BSE signal contrast is indicative of compositional differences—bright and dark areas indicate high and low atomic number materials, respectively. For example, kerogen and bitumen show up as dark gray regions while their chemically and spatially associated pyrite crystals are bright white, therein affording a means to readily differentiate these low and high atomic number components from the rest of the complex, intermediate atomic number mineral milieu (e.g., Figure 3). Nonetheless, the lower grayscale contrast among these other constituents and the overall compositional heterogeneity of shale specimens present a significant challenge to BSE studies of shale geochemical and microstructural relationships alone. Although the advent of EDS elemental mapping has

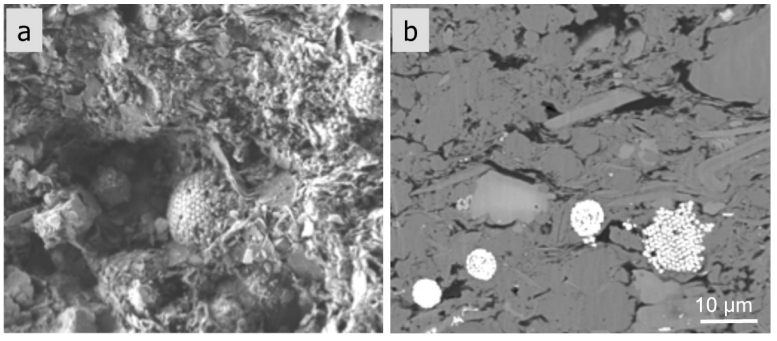

Figure 2. Field emission scanning electron microscope (FE-SEM) images of Marcellus shale specimen before (left) and after (right) ion beam milling. The image on the left was taken with an Everhart-Thornley secondary electron detector and shows a substantial amount of relief associated with mechanical abrasion. The image on the right shows a smooth, flat surface following ion milling.

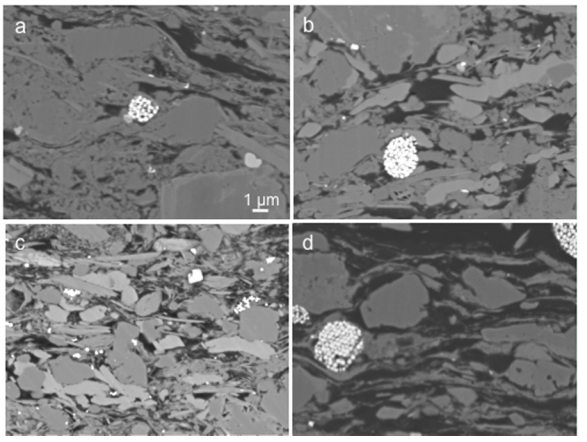

Figure 3. Backscatter field emission scanning electron microscope (FE-SEM) images of the specimens from four different formations: (a) Barnett, (b) Marcellus, (c) Haynesville, and (d) Woodford. All images were taken at 8 kV.

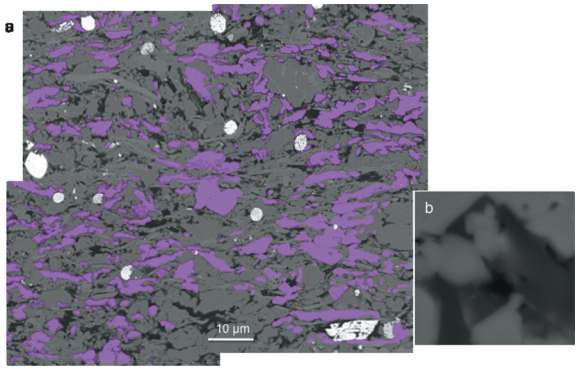

Figure 4. (a) Montage of 2 × 2 image tiles and corresponding energy-dispersive spectroscopy (EDS) maps of calcium (pink) distribution in the Marcellus shale. Both the backscattered electron (BSE) images and the EDS maps were acquired with high pixel resolution, so that the images can be later examined at higher magnification without loss of resolution. Data acquired at 8 kV using 50-mm^2 Oxford silicon drift detector (SDD). (b) A 2.5-µm^2 area zoom-in of BSE image showing organic matter (OM) and mineral porosity.

helped to further define these relationships (Figure 4), the low magnification required to yield a representative sampling area for compositional analysis obscures the corresponding nanoscale organic and mineral pore networks thought responsible for most petroleum storage and flow in shales. The user must therefore devise an approach that would combine these seemingly diverging needs into a single technique.

The acquisition of companion sets of high-pixel-resolution BSE and EDS images at low magnification is one such solution. For instance, low-magnification (e.g., ×2500) BSE images can be collected at 5000 × 4000 (5 × 4K) pixel resolution, allowing the image to be expanded to effectively ×12,500 without any significant loss of pixel resolution. The same can be done with EDS, wherein maps can be collected at up to 4 × 4K resolution. These data sets can then be integrated to simultaneously yield a broad overview of shale geochemical composition along with information on associated microstructural features. Alternatively, a series of neighboring high-magnification, high-pixel-resolution images and EDS maps can be acquired in automated fashion using current FE-SEM software and subsequently combined into a large-scale montage (see Ogura et al., 2010, for a case study using brain tissue). An example of 2 × 2 tiled BS montage images collected at 5 × 4K resolution (46 × 15 µm viewing area) for the Marcellus shale is shown in Figure 4a, along with corresponding EDS Ca Kα spectral overlays documenting the locations of calcite, dolomite, and aragonite. Figure 4b demonstrates how a 2.5-µm^2 portion of the same montage can be used to examine organic matter- and mineral-hosted porosity in more detail without any loss of resolution. This approach can be further utilized with more rigorous BSE/EDS segmentation algorithms to relate microscale compositional and structural features of shales to their macroscale petrophysical manifestations.

Using the methods described, some general microscale compositional and structural features can be delineated in each of the shale formations studied here. The siliceous Barnett, for example, displays abundant organic-matter-hosted pores with less mineral porosity, similar to previous observations (Loucks et al., 2009; Wang and Reed, 2009; Loucks et al., 2010; Milner et al., 2010; Sondergeld et al., 2010), whereas micrometer- to nanometer-size pores in the argillaceous Marcellus sample appear to be predominantly associated with organic-clay mineral interfaces as likewise reported by previous studies (Milner et al., 2010; Curtis et al., 2011a). These mixed-porosity systems are bracketed by the behavior of the calcareous Haynesville, for which the high level of thermal maturation (T_{max} = 512°C, VR_E = 2.4%) has led to a greater abundance of larger organic matter-hosted pores; and of the carbonaceous Woodford shale, in which a pore network has yet to clearly develop in its abundant yet thermally immature (T_{max} = 435°C, VR_E = 0.6%) organic matter inventory. Indeed, mineral-based pores (perhaps volumetrically dominated by diagenetic pyrite) may represent the only viable storage and migration pathway for oil and wet gas production from relatively low-maturity shale plays or sections of a play. In any case, these microscale descriptions are qualitatively consistent with bulk compositional and

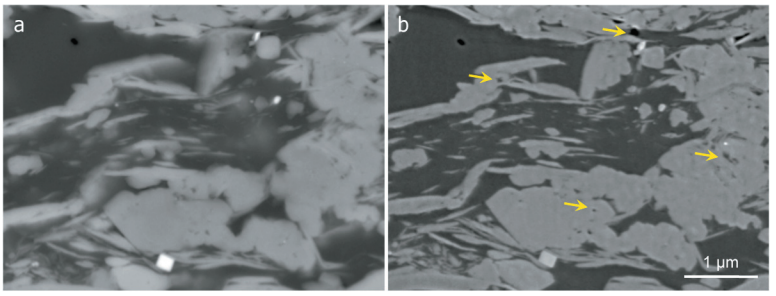

Figure 5. Comparison between (a) 8-kV and (b) 2-kV beam accelerating voltage observations of the Woodford shale specimen acquired across the same field of view. Arrows in (b) highlight pores that were previously obscured by a larger depth of investigation at 8 kV.

petrophysical properties measured on macroscale aliquots of the same material (Table 2). X-ray diffraction analysis, for example, indicates predominantly quartz, clay mineral, carbonate, and organic matter contents for the Barnett, Marcellus, Haynesville, and Woodford samples, respectively. In fact, the very high (23 wt%) *TOC* content of the Woodford as both measured by combustion EA and reflected at the SEM scale (Figure 3) is further expressed in a marked 0.5-g cm^{-3} depression in bulk density relative to its lower *TOC* counterparts (Table 2). Organic matter maturation also appears to play a dominant role in setting the comparatively high porosity of 11.8% measured for the Haynesville shale.

Given the reputed importance of organic pore networks for petroleum storage and flow in shale reservoirs (O'Brien et al., 1994, 2002; Javadpour, 2009; Loucks et al., 2009; Wang and Reed, 2009; Shabro et al., 2011), SEM has become an increasingly important tool to investigate their basic structure and distribution. Even so, their small size has typically demanded high accelerating voltages (i.e., $>$ 15 kV) coupled with BSE detection to achieve the nanometer-size feature resolution needed for accurate characterization. Yet the large volume of interaction (up to several cubic micrometers) produced at high acceleration voltages along with the low BSE grayscale contrast between these pores and the surrounding organic matter matrix can lead to subjective segmentation workflows. New developments in FE-SEM technology (e.g., Erdman et al., 2009, 2010) allow the user to maintain single-nanometer spatial resolution while imaging the specimen and performing microanalysis at lower accelerating voltages to reduce the interaction volume and improve surface contrast. Figure 5 shows a comparison of BSE images taken at 8 and 2 kV for the same Woodford shale specimen. The arrows point to features observed at 8 kV that completely disappear at 2 kV following reduction in the beam-specimen interaction volume. This behavior can also be modeled by utilizing the Monte Carlo simulations (Hovington et al., 1997) of beam interaction with carbon, silicon, and

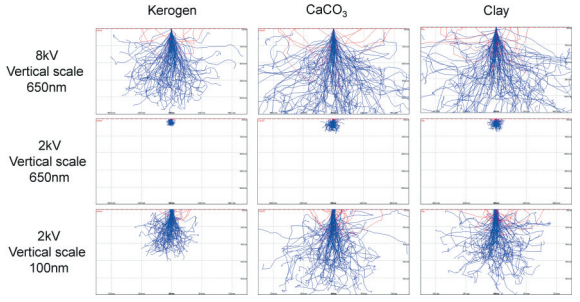

Figure 6. Monte Carlo simulations (CASINO®) of secondary (blue) and backscattered (red) electron beam-specimen interactions in three components of shale (organic matter [OM], calcite, and clay minerals) at both high (8-kV) and low (2-kV) beam accelerating voltages. Note greater interaction volume at higher voltage. $CaCO_3$ = calcium carbonate.

calcium (as rough proxies for organic matter, quartz, and calcite, respectively) at 8 and 2 kV (Figure 6).

Utilization of low beam voltages also reduces radiation damage to the shale structure itself. For example, our experience demonstrated that morphologically distinct calcite fragments have been shown to be susceptible to degradation under a 5-kV beam but encumber no apparent alteration at only 2 kV. Nonetheless, companion EDS mapping of all major elemental constituents of shale (i.e., silicon, calcium, aluminum, magnesium, potassium, sodium, iron, sulfur, oxygen, and carbon) still requires the collection of x-ray spectra across energies of up to approximately 8 kV depending on whether K or L x-ray lines are used for identification and quantification. For this application, care should thus be taken to minimize the amount of time shale samples are exposed to high beam currents and accelerating voltages by employing a large, high-efficiency SDD.

Complimentary information on shale elemental composition can sometimes be obtained at lower voltages and superior resolution using SEM-mounted CL detectors. In CL, the interaction of the primary electron beam with the specimen results in the promotion

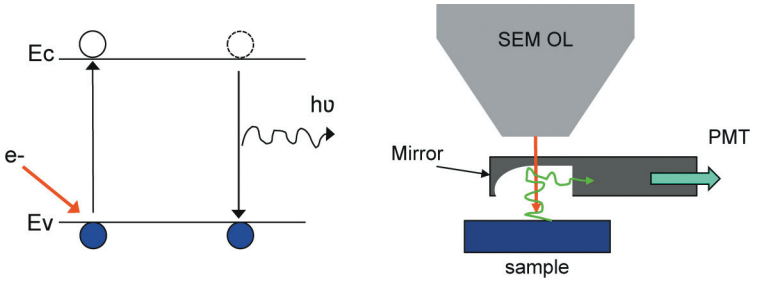

Figure 7. KE Centaurus cathodoluminescence (CL) images (left), overlaid backscattered electron (BSE) images-EDS (energy-dispersive spectroscopy) maps (center), and remaining EDS surveys (right) of the Woodford sample, all acquired at 5-kV accelerating voltage.

of valence band electrons to the conduction band. Subsequent relaxation emits photons whose energies are characteristic of particular elemental constituents or mineral defects. These photons are then collected by an elliptical mirror, separated by a monochromator (if present), and detected by a PMT to render composite grayscale or spectrally resolved compositional information across a sample surface. Similar to EDS, the use of CL can therefore aid in the differentiation between various materials of different CL characteristics but similar electron backscatter coefficient (i.e., minimal difference in backscatter image contrast) (Erdman et al., 2009, 2010; Sondergeld et al., 2010). For example, the calcite, dolomite, and quartz constituents of shale studied here have distinctly bright CL signatures relative to less optically active components like clay minerals or organic matter. Moreover, CL has been previously demonstrated to be capable of discriminating finely crystalline, low-permeability dolomites from coarser, higher-permeability morphotypes as well as primary from authigenic quartz (Boggs and Krinsley, 2006). With this in mind, combined application of CL and EDS technology (Figure 7) promises to further uncover the microscale geochemical-microstructural relationships that underpin macroscale petrophysical properties of unconventional shale systems.

SUMMARY AND PERSPECTIVE

The addition of CP preparation to standard shale SEM imaging workflows over the past several years has revolutionized the microscale characterization of shale fabric (i.e., the distribution and association of organic, mineral, and pore constituents) that is likely to strongly influence petroleum storage and flow therein. The concomitant integration of more diverse yet complimentary detection systems such as CL and EDS along with the optimization of traditional detectors (SE and BSE) has lent further insight into the fundamental geochemical controls on microstructural properties in shales, not the least of which is the development of organic-matter-hosted nanopores on thermal maturation. Although focused ion milling combined with ever-more-sophisticated image alignment/segmentation software has garnered more recent attention because of its ability to render true three-dimensional (3-D) reconstructions of shale matrices (e.g., Elgmati et al., 2011a, b), the nanometer- to micrometer-level areas of investigation to which this technique is confined (along with the high cost of acquisition) has so far limited its widespread use in shale research. Future developments should therefore focus on comparing the upscaling potential of two-dimensional versus 3-D microscale information to core or wellbore log measurements as well as integrating SEM instrumentation with dynamic experiments such as hydraulic fracturing, multiphase fluid imbibition, and pyrolytic artificial maturation.

ACKNOWLEDGMENTS

We thank the TerraTek core analysis team for providing the bulk porosity, density, mineralogy, and vitrinite reflectance data along with the SDR Petrolabs staff for additional sample preparation. Maria Mastalerz of Indiana University generously supplied the bitumen reflectance value for the Haynesville sample. Regina Campbell of JEOL is also acknowledged for help with SEM sample preparation.

REFERENCES CITED

Behar, F., V. Beaumont, and H. L. De B. Penteado, 2001, Rock-Eval 6 technology: Performances and developments: Oil & Gas Science and Technology, v. 56, no. 2, p. 111–134.

Boggs, S., and D. Krinsley, 2006, Application of cathodoluminescence imaging to the study of sedimentary rocks: Cambridge, Cambridge University Press, 176 p.

Brodie, C. R., M. J. Leng, J. S. L. Casford, C. P. Kendrick, J. M. Lloyd, Z. Yongqiang, and M. I. Bird, 2011, Evidence for bias in C and N concentrations and $\delta^{13}C$ composition of terrestrial and aquatic organic materials due

to pre-analysis acid preparation methods: Chemical Geology, v. 282, p. 67–83.

Bustin, A. M. M., and R. M. Bustin, 2008, Importance of fabric on the production of gas shales: Society of Petroleum Engineers Unconventional Reservoirs Conference, February 10–12, Keystone, Colorado, SPE Paper 114167, 29 p., doi: 10.2118/114167-MS.

Curtis, M. E., R. J. Ambrose, C. H. Sondergeld, and C. S. Rai, 2010, Structural characterization of gas shales on the micro- and nano-scales: Canadian Society for Unconventional Gas/Society of Petroleum Engineers Canadian Unconventional Resources and International Petroleum Conference, October 19–21, Calgary, Alberta, SPE Paper 137693, 15 p., doi: 10.2118/137693-MS.

Curtis, M. E., R. J. Ambrose, C. H. Sondergeld, and C. S. Rai, 2011a, Investigation of the relationship between organic porosity and thermal maturity in the Marcellus shale: Society of Petroleum Engineers North American Unconventional Gas Conference and Exhibition, June 14–16, The Woodlands, Texas, SPE Paper 144370, 4 p., doi: 10.2118/144370-MS.

Curtis, M. E., R. J. Ambrose, C. H. Sondergeld, and C. S. Rai, 2011b, Transmission and scanning electron microscopy investigation of pore connectivity of gas shales on the nanoscale: Society of Petroleum Engineers North American Unconventional Gas Conference and Exhibition, June 14–16, The Woodlands, Texas, SPE Paper 144391, 10 p., doi: 10.2118/144391-MS.

Dacy, J. M., 2010, Core tests for relative permeability of unconventional gas reservoirs: Society of Petroleum Engineers Annual Technical Conference and Exhibition, September 19–22, Florence, Italy, SPE Paper 135427, 18 p., doi: 10.2118/135427-MS.

Elgmati, M., H. Zhang, B. Bai, and R. Flori, 2011a, Submicron-pore characterization of shale gas plays: Society of Petroleum Engineers North American Unconventional Gas Conference and Exhibition, June 14–16, The Woodlands, Texas, SPE Paper 144050, 19 p., doi: 10.2118/144050-MS.

Elgmati, M., M. Zobaa, H. Zhang, B. Bai, and F. Oboh-Ikuenobe, 2011b, Palynofacies analysis and submicron pore modeling of shale-gas plays: Society of Petroleum Engineers North American Unconventional Gas Conference and Exhibition, June 14–16, The Woodlands, Texas, SPE Paper 144267, 10 p., doi: 10.2118/144267-MS.

Erdman, N., R. Campbell, and S. Asahina, 2006a, Argon beam cross sectioning: Advanced Materials and Processes, v. 164, no. 6, p. 33–35.

Erdman, N., R. Campbell, and S. Asahina, 2006b, Precise SEM cross section polishing via argon beam milling: Microscopy Today, v. 14, no. 3, p. 22–25.

Erdman, N., N. Kikuchi, A. Laudate, and V. Robertson, 2009, Multispectral imaging in a FEG-SEM: Advanced Materials and Processes, v. 167, no. 9, p. 28–31.

Erdman, N., N. Kikuchi, R. Campbell, and V. E. Robertson, 2010, SEM technology advances energy research: Advanced Materials and Processes, v. 168, no. 2, p. 14–15.

Handwerger, D. A., R. Suarez-Rivera, K. I. Vaughn, and J. F. Keller, 2011, Improved petrophysical core measurements on tight shale reservoirs using retort and crushed samples: Society of Petroleum Engineers Annual Technical Conference and Exhibition, October 30–November 2, Denver, Colorado, SPE Paper 147456, 12 p., doi: 10.2118/147456-MS.

Hovington, P., D. Drouin, and R. Gauvin, 1997, CASINO: A new era of Monte Carlo code in C language for the electron beam interaction—Part I: Description of the programme: Scanning, v. 19, p. 1–14.

Javadpour, F., D. Fisher, and M. Unsworth, 2007, Nanoscale gas flow in shale sediments: Journal of Canadian Petroleum Technology, v. 46, no. 10, p. 55–61.

Javadpour, F., 2009, Nanopores and apparent permeability of gas flow in mudrocks (shales and siltstone): Journal of Canadian Petroleum Technology, v. 48, no. 8, p. 16–21.

Loucks, R. G., R. M. Reed, S. C. Ruppel, and D. M. Jarvie, 2009, Morphology, genesis, and distribution of nanometer-scale pores in siliceous mudstones of the Mississippian Barnett shale: Journal of Sedimentary Research, v. 79, p. 848–861.

Loucks, R. G., R. M. Reed, S. C. Ruppel, and U. Hammes, 2010, Preliminary classification of matrix pores in mudrocks: Gulf Coast Association of Geological Societies Transactions, v. 60, p. 435–441.

Milner, M., R. McLin, and J. Petriello, 2010, Imaging texture and porosity in mudstones and shales: Comparison of secondary and ion-milled backscatter SEM methods: Canadian Society for Unconventional Gas/Society of Petroleum Engineers Canadian Unconventional Resources and International Petroleum Conference, October 19–21, Calgary, Alberta, SPE Paper 138975, 10 p., doi: 10.2118/138975-MS.

O'Brien, N. R., R. M. Slatt, and J. Senftle, 1994, The significance of oil shale fabric in primary hydrocarbon migration: Fuel, v. 73, no. 9, p. 1518–1522.

O'Brien, N. R., M. D. Cremer, and D. G. Canales, 2002, The role of argillaceous rock fabric in primary migration of oil: Gulf Coast Association of Geological Societies Transactions, v. 52, p. 1103–1112.

Ogura, K., M. Kamidaira, S. Asahina, and N. Erdman, 2007, New methods for cross-section sample preparation using broad argon ion beam: Microscopy and Microanalysis, v. 13, p. 1518–1519.

Ogura, K., M. Yamada, O. Hirahara, M. Mita, N. Erdman, and C. Nielsen, 2010, Gigantic montages with a fully automated FE-SEM (serial sections of a mouse brain tissue): Microscopy and Microanalysis, v. 16, p. 52–53.

Passey, Q. R., W. L. Bohacs, R. Esch, R. Klimentidis, and S. Singha, 2010, From oil-prone source rock to gas-producing shale reservoir—Geologic and petrophysical characterization of unconventional shale-gas reservoirs: Society of Petroleum Engineers International Oil and Gas Conference and Exhibition in China, June 8–10, Beijing, China, SPE Paper 131350, 29 p., doi: 10.2118/131350-MS.

Ross, D. K. J., and R. M. Bustin, 2009, The importance of shale composition and pore structure upon gas storage potential of shale gas reservoirs: Marine and Petroleum Geology, v. 26, p. 916–927.

Ruessink, B. H., and D. G. Harville, 1992, Quantitative analysis of bulk mineralogy: The applicability and performance of XRD and FTIR: Society of Petroleum Engineers Formation Damage Control Symposium, February 26–27, Lafayette, Louisiana, SPE Paper 23828, 14 p., doi: 10.2118/23828-MS.

Schieber, J., 2001, A role for organic petrology in integrated studies of mudrocks: Examples from Devonian black shales of the eastern U.S.: International Journal of Coal Geology, v. 47, p. 171–187.

Shabro, V., C. Torres-Verdin, and F. Javadpour, 2011, Numerical simulation of shale-gas production: From pore-scale modeling of slip-flow, Knudsen diffusion, and Langmuir desorption to reservoir modeling of compressible fluid: Society of Petroleum Engineers North American Unconventional Gas Conference and Exhibition, June 14–16, The Woodlands, Texas, SPE Paper 144355, 11 p., doi: 10.2118/144355-MS.

Sondergeld, C. H., R. J. Ambrose, C. S. Rai, and J. Moncrieff, 2010, Micro-structural studies of gas shales: Society of Petroleum Engineers Unconventional Gas Conference, February 23–25, Pittsburgh, Pennsylvania, SPE Paper 131771, 17 p., doi: 10.2118/131771-MS.

Sun, W., J. E. Andrade, J. W. Rudnicki, and P. Eichhubl, 2011, Connecting microstructural attributes and permeability from 3D tomographic images of in situ shear-enhanced compaction bands using multiscale computations: Geophysical Research Letters, v. 38, doi: 10.1029/2011GL047683.

Wang, F. P., and R. Reed, 2009, Pore networks and fluid flow in gas shales: Society of Petroleum Engineers Annual Technical Conference and Exhibition, October 4–7, New Orleans, Louisiana, SPE Paper 124253, 8 p., doi: 10.2118/124253-MS.